Soft Matter

Adhesion and Mechanical Properties of Poly(dimethyl siloxane) Bottlebrush Elastomers

Journal:	*Soft Matter*
Manuscript ID	SM-ART-03-2023-000346.R1
Article Type:	Paper
Date Submitted by the Author:	16-Jun-2023
Complete List of Authors:	Kim, Hyemin; University of Massachusetts Amherst, Watkins, James; University of Massachusetts Amherst, Polymer Science and Engineering Crosby, Alfred; University of Massachusetts, Polymer Science and Engineering

Adhesion and Mechanical Properties of Poly(dimethyl siloxane) Bottlebrush Elastomers

Hyemin Kim, James J. Watkins, and Alfred J. Crosby**

Department of Polymer Science and Engineering, University of Massachusetts Amherst, Amherst, Massachusetts 01003, United States

* Corresponding Authors Email: watkins@polysci.umass.edu (J.J. Watkins) and crosby@mail.pse.umass.edu (A.J. Crosby)

Keywords poly(dimethylsiloxane), bottlebrush, elastomer, adhesion, interfacial, softness, relaxation, rate dependence

Abstract

Poly(dimethyl siloxane) (PDMS) bottlebrush elastomers (BBEs) are attractive soft materials with well-controlled bulk mechanical properties. However, their surface and interfacial properties have not been studied in depth. We report a detailed study of the adhesion of PDMS BBEs to glass using a contact adhesion test to determine the critical energy release rates, $\boldsymbol{G_c}$, as a function of interfacial separation velocity. For BBEs, $\boldsymbol{G_c}$ for initiating separation, $\boldsymbol{G_0}$, was found to be independent of the crosslink density. We hypothesize that the monomer chemistry of side chains plays a primary role in defining surface properties for this materials system. After crack initiation, BBEs showed a significantly lower $\boldsymbol{G_c}$ and less velocity dependence than linear chain networks. Scaling analysis attributes these properties to the faster dissipative relaxation mechanisms within the BBEs. These findings demonstrate that the adhesion properties of BBEs can be finely tuned through the

monomer chemistry and side chain length for potential applications.

1. Introduction

Bottlebrush elastomers (BBEs) are promising super-soft materials for applications ranging from wearable electronics to biomedical devices.[1-5] Their densely grafted side chains cause steric repulsions and suppress chain entanglements, resulting in super-softness (1 kPa < elastic modulus, E < 100 kPa).[6-8] Other soft materials, such as hydrogels or organogels, typically rely upon free small molecules including solvents or water to decrease the density of crosslink junctions within their three-dimensional networks to achieve equivalent low elastic moduli. With BBEs, low moduli, which approach the moduli of many soft biological tissues, can be achieved without the need for "free" molecules or components, which are not chemically bound to the network. Such free components can cause the material to have unstable or transient properties, or pronounced viscoelasticity, which can be undesirable for many soft materials technologies.

BBEs have three key independent architectural parameters: the degrees of polymerization 1) of side changes (n_{sc}), 2) between neighboring side chains (n_g), and 3) between neighboring crosslinks

(n_x) (**Figure 1(a)**). Their bulk mechanical properties are controlled by these three parameters. [4, 6, 7, 9] These relationships are well-investigated experimentally, as well as through molecular dynamics simulations for various chemistries.[4, 9-11] However, there are limited studies on their surface and interfacial properties, especially adhesion properties.

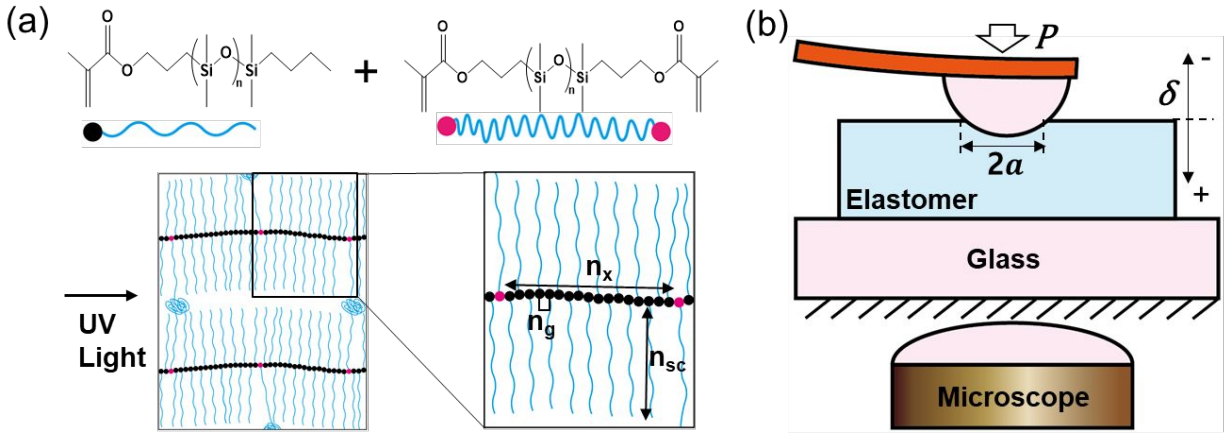

Figure 1. **(a)** PDMS bottlebrush elastomers (BBEs) prepared by free radical photo-polymerization with the degrees of polymerization of side changes (n_{sc}), between neighboring side chains (n_g), and between neighboring crosslinks (n_x). **(b)** Schematic of a contact adhesion test used to measure the applied load ($\boldsymbol{P}$), displacement ($\boldsymbol{\delta}$), and radius ($\boldsymbol{a}$) of the contact area between the glass probe and elastomers.

PDMS BBEs hold great potential offering advanced control of adhesion. Their extended side chain architecture provides a path for achieving ultra-low elastic moduli, which decreases the energy cost of forming interfaces with complex geometries. Forming interfacial contact is a primary objective for any adhesion-based application. Traditionally, adhesive materials are formulated with small molecule additives within crosslinked and entangled networks in order to enhance mobility and decrease the energetic cost of forming an interface over time. However, this design approach also complicates the engineering of soft interfaces due to the complex, time dependent properties that the small molecule additives impart. Based on the architectural design of BBEs, the formation of intimate interfacial contact should be possible with minimal time dependence. Furthermore, PDMS BBEs are particularly attractive since their anticipated low surface energy should allow interfaces to be separated easily when loads are concentrated. If they have minimal time dependent adhesion mechanisms, then interfacial separation is potentially more straightforward to engineer for applications that require minimal damage and reversibility.

To this end, the adhesion of PDMS BBEs has been studied to a limited extent. For example,

Duncan *et al* used PDMS BBEs to remove soil particulates without damaging underlying substrates.[3] Cai *et al* also characterized the interfacial fracture energy of PDMS BBEs and steel interfaces.[12] Though these studies introduced some of the potential attractive adhesion properties of PDMS BBEs, they have not provided a detailed understanding of these properties and how they may relate to the molecular architecture.

Herein, we report a detailed study of the mechanical properties of PDMS BBEs and their adhesion with glass via JKR-based contact adhesion test. This approach allows us to separate bulk and surface contributions[13-16], thus providing insight into the unique attributes of PDMS BBEs and how to utilize them for desired applications. We used radical polymerized PDMS BBEs and varied the average degree of polymerization between crosslinks to understand its role in adhesion. Their softness was controlled by the crosslinking density. The effects of molecular architecture on interfacial interactions and energy dissipation were assessed by comparing the properties of PDMS BBEs with those of commercially-available PDMS networks composed of linear polymers. Our findings reveal that the zero-velocity adhesion of PDMS BBEs to glass is more than an order of magnitude less than that with PDMS linear chain networks and that the velocity dependence of

both network architectures is similar. We discuss the structure-property mechanisms underlying these findings and propose how these properties may be used in the design of robust, reversible soft adhesives.

2. Experiments

2.1 Preparation of Elastomers

Monomethacryloxypropyl-terminated polydimethylsiloxane (monomer; MCR-M11) and methacryloxypropyl terminated polydimethylsiloxane (crosslinker; DMS-R18) were purchased from Gelest. Macromonomers were passed through basic alumina to remove the inhibitor before radical polymerization. Photo-initiator (2-hydroxy-2-methylpropiophenone, Darocur 1173, BASF) was used as received. Crosslinking density was controlled by molar ratios of crosslinker (φ_x) ranging from 1.5 to 3.6 mol%. Targeted n_x are calculated from $n_x = 1/(2\varphi_x)$.[1] The solution of 1.1 mol% initiator, monomer, and crosslinker were mixed homogeneously by stirring, poured into a round mold with a diameter of 40 mm, and cured under N_2 with a high-pressure ultraviolet lamp

(USH508SA, Ushio, 6.1 mW·cm^{-2} at 365 nm) for six hours. After polymerization, elastomers were immersed in acetone three times over two days to remove unreacted monomers and crosslinkers, then samples were de-swollen in ethanol for eight hours and vacuum-dried at 40 ˚C overnight. Dried BBEs were transparent and 2.3 mm thick. Their gel fractions were highly reproducible and determined to range from 86.2±0.4% to 88.3±0.4% depending upon their n_x (**Figure S3**). These measurements are made by comparing the mass of the dried elastomer before extraction and after extraction. BBEs were punched by a hollow metal punch into a circular shape with a diameter of 13 mm for instrumental measurements. As a methacrylate group of monomers consists of one unit of backbone in the bottlebrush networks, the backbone is poly (methylmethacrylate) (PMMA) and $n_g = 1$. The length of PDMS side chains, n_{sc} is 14 for all BBEs while n_x is 17, 25, and 34 depending on the crosslinker mole fraction, φ_x.[1] For more reliable calculations of φ_x and n_x, the molecular weight, $M_{n,}$ and polydispersity of macromonomers were characterized by ^{1}H NMR and GPC (**Figure S1 – 3, Table S1**). Based on the volume fraction of backbone monomers and the length of side chains (**Table S2**), these BBEs belong to the stretched side chain (SSC) regime in the diagram of states of graft copolymers.[6, 8, 17] In this regime, all side chains stretch to satisfy the monomer

packing condition. The softness of BBEs is well-controlled with n_x and the elastic modulus has a linear relationship with the inverse of n_x like previous studies[4, 10, 17] (**Figure S5 (a)**). BBEs samples are named n_x = #, in which # represents the average degree of polymerization between crosslinks.

Linear PDMS elastomers were prepared from Sylgard 184 (Dow), and the weight ratios of the base resin to curing agent were 40: 1, 50: 1, and 55: 1 for the cured elastomers to have comparable moduli to the BBEs (**Figure S5 (b)**). For the PDMS linear chain networks, the mixed formulations were poured into plastic Petri dishes and cured at 70 ˚C for 24 hours. After curing, the sol fraction was extracted following the same extraction process as used for the BBEs. The thickness of these Sylagard-based materials was approximately 2.5 mm, and the gel fraction ranged from 83.4±0.9 % to 85.6±0.5 % depending upon their formulation (**Table S3)**. The sample name is abbreviated with "Syl#", in which # represents the ratio of the base per curing agent.

The mechanical response of the aforementioned BBEs and linear chain networks was dominated by the density of covalent crosslinks. Though trapped entanglements in polymer networks can significantly impact mechanical properties[18-20], the extent of entanglements in the BBEs studied here was assumed to be negligible based on previous experimental and scaling analysis.[17]

Furthermore according to the multi-angle laser light scattering (MALLS) results (**Figure S4**), the molar mass of the uncrosslinked PDMS bottlebrush polymer was 2.92 x 10^5 $gmol^{-1}$ and PDI of it was 1.92, which is much lower than the previously reported molar mass of the entanglement strands, M_e, of PDMS bottlebrush polymer with the same n_g and n_{sc}.[21] For the linear chain networks, the measured elastic moduli, which are less than 70 kPa, are below the lower limit set by entanglements for conventional linear polymers. Accordingly, we assume that the extent of trapped entanglements in the linear polymer networks is negligible, likely due to the excess free molecules associated with the polymerization conditions used here.[22]

2.2 Dynamic Mechanical Analysis (DMA)

Rheological properties of elastomers were characterized with a Discovery DMA 850 (TA Instruments) at room temperature. The cylindrical sample with a diameter of 13 mm and a thickness of 2.3 – 2.5 mm was placed within the compression clamps. Storage moduli (E'), loss moduli (E''), and tan δ (= E''/E') were measured with varying strain from 0.1% to 8 % at a fixed frequency of 1 Hz (**Figure S7**) and with varying frequency from 0.01 Hz to 100 Hz at a fixed strain of 1 % (**Figure S8 and S9**). Preload of 0.1 N was applied to ensure good contact with the clamps.

To probe the relaxation time of bottlebrush networks, frequency sweep tests at low temperatures of -50 and -75 ˚C were conducted for time-temperature superposition (**Figure S10**).

2.3 Contact Adhesion Test (CAT)

Contact adhesion tests (CAT) were used to reveal the adhesion properties between a glass probe and elastomers. **Figure 1 (b)** is a schematic of the contact adhesion test used to measure the applied load ($\boldsymbol{P}$), displacement ($\boldsymbol{\delta}$), and radius ($\boldsymbol{a}$) of the contact area between the glass probe and elastomers. A hemispherical glass probe with a radius of 2.5 mm approached a sample until the resultant contact load reached 10 mN, and then the probe retracted until final interfacial separation occurred. The load cell and nanopositioner were connected to the probe to collect $\boldsymbol{P}$ and $\boldsymbol{\delta}$ during the measurement. The contact images were taken by the optical microscope through the glass substrate and elastomers. The radius of the contact area in each image was determined using the image analysis program, Image J. CAT experiments were performed on three individual samples of each composition, and displacement rates of the indenter were 1, 10, and 100 μm/sec. The glass probe was cleaned with isopropyl alcohol after each run.

The adhesion of elastomers on a glass probe is quantified by the energy release rate, G_c at each data point during measurement (Eq S1).[13-16, 23] When the probe retracts from the soft surface during unloading, the contact radius decreases with the crack velocity, v. G_c is empirically known to be a function of v with three materials-defined parameters, G_0, n, and v^*, attributed to adhesion properties of the material:

$$G_c = G_0\left(1 + \left(\frac{v}{v^*}\right)^n\right) \qquad \text{(Eq 1)}$$

where v is $-\frac{da}{dt}$. The zero-velocity adhesion, G_0, is the critical energy release rate to initiate separation. After G_c overcomes G_0, the interfacial crack begins to propagate. The velocity dependence of adhesion is described by the empirical values of characteristic velocity, v^* and the velocity exponent, n. These are dependent on bulk energy dissipation within the soft materials during detachment. For elastomers, the exponent, n is typically found to be 0.6.[24, 25]

In addition to G_c, the data from CAT measurements are used to quantify the elastic modulus, E, by the least square fitting of the measured load and calculated load by JKR model (Eq S2 – 5). This value of the elastic modulus assumes quasi-elastic conditions for the fixed displacement rate

used in the CAT measurements. Additionally, the work of adhesion, W_{adh} is determined from the hysteresis of the load-displacement curves during unloading divided by the maximum contact area.

3. Results and discussion

Figure 2 (a) shows load-displacement curves of PDMS BBEs during representative CAT measurements at a fixed displacement rate. While the probe rate changes with 1, 10, and 100 μm/sec, the loading curves of each sample overlap, with the slope governed by the stiffness of the BBEs. The slope gradually decreases as n_x increases from 17 to 34. On the other hand, the degree of hysteresis and maximum tensile force increase with faster probe rates. This rate dependence is typical for viscoelastic materials.[26] During the detachment of the glass indenter from elastomers, energy is released by the viscous component of soft elastomers. Therefore its contribution to adhesion is reflected in the dependence on the displacement rate.[27, 28] These rate-dependent behaviors are also observed in linear chain networks; in fact, the amount of hysteresis and the

maximum force of separation are considerably larger as compared to the BBEs (**Figure S5**). All of the BBEs and linear chain networks keep a circular shape of contact area without cavitation or fingering during the loading and unloading process (**Figure 2 (b)**).

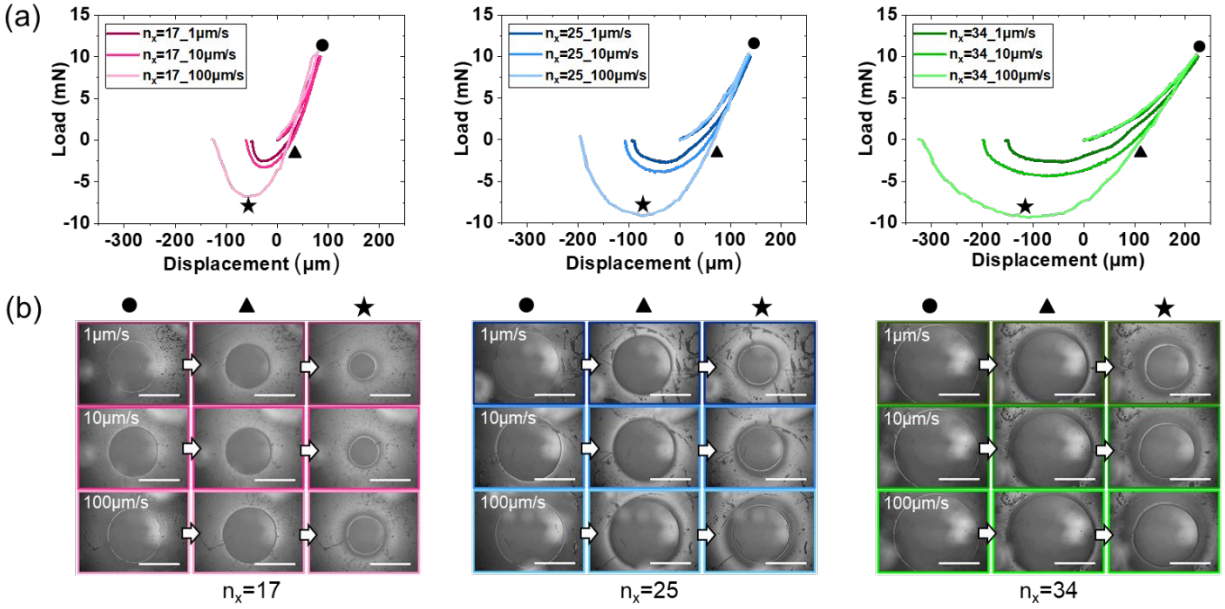

Figure 2. (a) Load-displacement curves of BBEs of n_x=17, 25, and 34 with three displacement rates of the probe (1, 10, and 100 μm/sec) **(b)** Contact images corresponding to marked points on (a); ● (load = 10 mN), ▲ (load = 0 mN), ★ (load = minimum value); scale bar is 500 μm.

The elastic modulus, E, as determined by the CAT measurements was well-controlled by the

crosslinking density. For BBEs, E decreased from 93 kPa to 17 kPa with the increase of n_x. For the linear chain networks, E decreased from 68 kPa to 11 kPa as the amount of base resin increased. For both elastomers, E did not significantly change with the displacement rate of the crosshead (**Figure 3 (a)**). Unlike the rate independence of E, the work of adhesion W_{adh} increased as the displacement rate was faster (**Figure 3 (b)**). The values of W_{adh} of BBEs ranged from 0.10 to 0.75 J/m^2 and are an order of magnitude less than those of linear elastomers, which ranged from 1.21 to 14.34 J/m^2 over all test conditions. Hence the BBEs are significantly less adhesive compared to the linear chain networks even though both have similar stiffness.

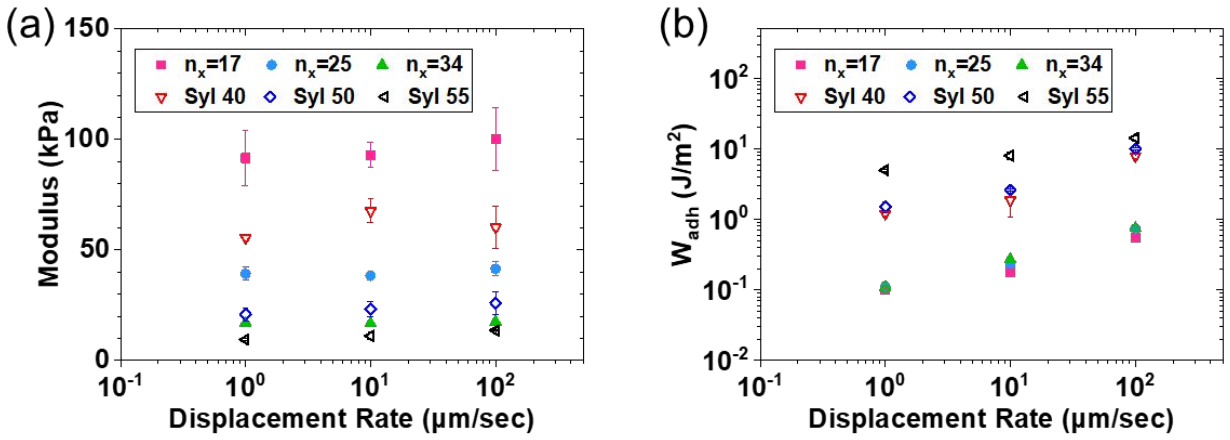

Figure 3. (a) Elastic moduli, E, and **(b)** work of adhesion, W_{adh}, of BBEs and linear chain networks with varying

displacement rates.

For further understanding of adhesion properties, G_c was plotted as a function of the crack velocity, v (**Figure 4**). It is clear that linear chain networks have significantly higher G_c values and larger velocity dependence in comparison with BBEs. To separate interfacial and bulk contributions to adhesion, G_0 and v^* values were determined by linear regression fitting from experimental values of G_c, with an assumed value of n=0.6 (**Table S4, and S5**). In the case of linear chain networks, as the elastomer gets softer G_0 increases from 0.48 to 1.31 J/m^2. However, interestingly, all BBEs have very small and modulus-independent G_0 of about 0.18 J/m^2. This finding suggests that the densely grafted and extended polymeric side chains of BBEs lead to similar adhesion properties regardless of the stiffness. In other words, these materials require the same amount of energy to initiate separation regardless of crosslink density. This finding is unusual for typical soft materials and is matched qualitatively with the previous study that found that the side chains of BBEs dictate surface properties in the context of antifouling or stimuli-responsive surface coatings.[29]

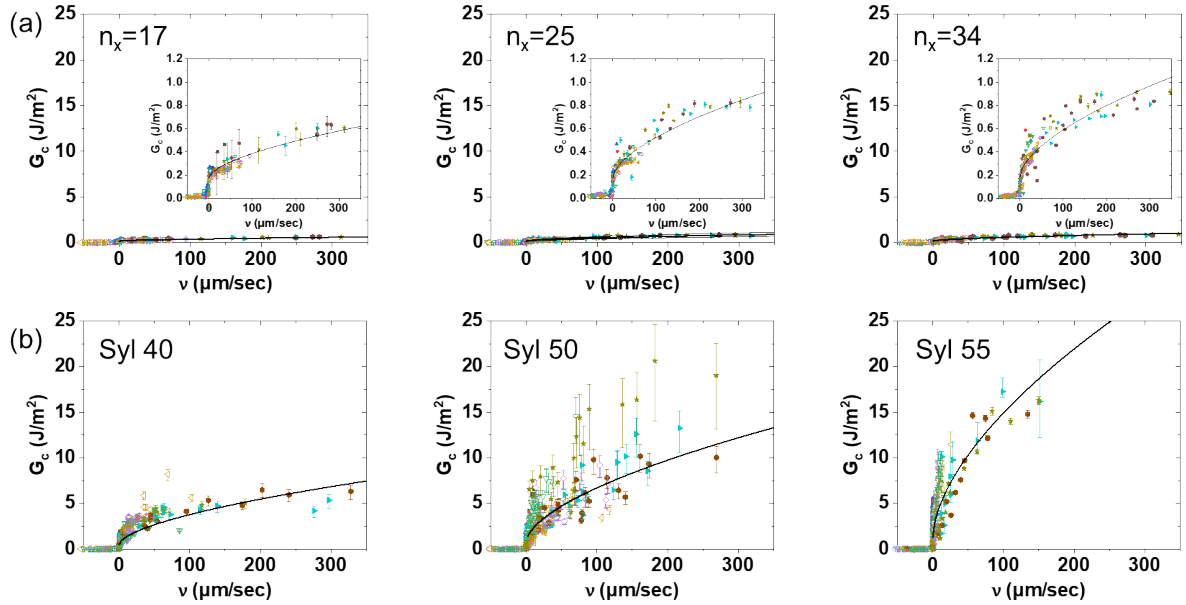

Figure 4. Plots of energy release rate, G_c and crack velocity, v of **(a)** BBEs and **(b)** linear chain networks. Insets of (a) are enlarged plots since the axes limits of non-inset plots are constant to emphasize contrast in the properties for the BBEs and linear chain networks. Data points represent the calculated G_c and v for each run (■,●,▲: probe velocity = 1 μm/sec; ▽,◇,◁ : 10 μm/sec; ▸, ⬣, ★: 100 μm/sec). The lines represent the linear regression fit to the data. The bold line is the representative prediction line when $G_c = G_0(1 + \left(\frac{v}{v^*}\right)^{0.6})$.

As v increases, G_c for linear elastomers increases significantly while that for BBEs rises slightly. This velocity dependence is described by the materials-defined parameter, v^*. For the linear elastomers, v^* decreases from 4.1 to 2.0 μm/sec; however, for BBEs v^* is considerably

larger and decreases from 77.7 to 27.1 μm/sec indicating much less velocity dependence. For example, Syl50 has a modulus of 23 kPa and v^* of 3.7 μm/sec while n_x=34 of BBEs with a modulus of 17 kPa has a higher v^* of 27.1 μm/sec.

This weak velocity dependence of BBEs is attributed to their bulk energy dissipation properties, which are frequency independent over a large range of frequencies. In **Figure 5**, BBEs show contrasting tan δ behaviors over a wide frequency of 0.01 – 100 Hz compared to linear chain networks. As tan δ is the ratio of the viscous to elastic contributions of an elastomer's viscoelastic properties, low and steady tan δ values of BBEs lead to a small and stable bulk energy release during detachment, showing less velocity dependence. The average strain rate for CAT measurements can be roughly estimated as the displacement rate (1,10, and 100 μm/sec) divided by the contact radius when the radius of contact is less than the thickness of the elastomer. Considering the maximum radii of the contact area are from 610 to 1150 μm depending upon the softness (**Figure S6**), the frequency range of the DMA-measured tan δ corresponds to the investigated strain rate of the CAT measurements. In addition, G_0 for the linear networks, 0.48 J/m^2 – 1.31 J/m^2 (**Table S5**), is larger than the typical thermodynamic work of adhesion, ~0.1 J/m^2,

for elastomers[15], suggesting that this parameter is still capturing some dissipative relaxation processes for the linear network materials.

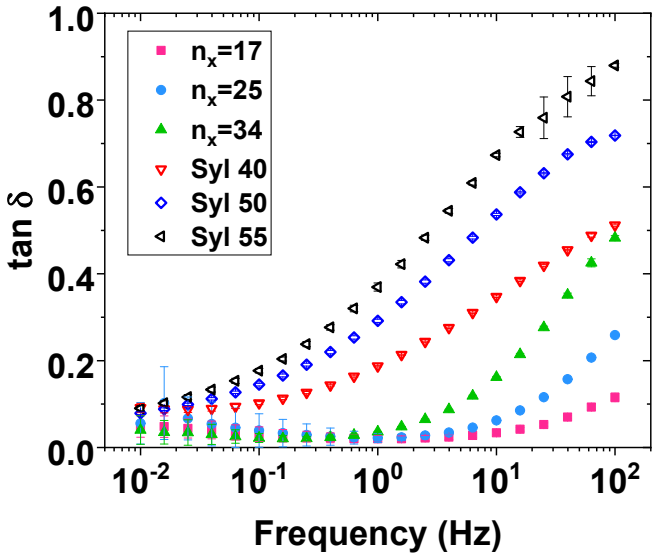

Figure 5. Frequency dependence of tan δ of BBEs and linear chain networks

We further investigated the network relaxation time, τ_{BB}, of the BBEs to probe the origins of bulk energy dissipation. τ_{BB} was determined from the inverse of the frequency at the crossing point, ω_{BB}, in the plot of E' and E'' as a function of the frequency (**Figure S10** and **Table S6**). A plot of τ_{BB} and n_x^2 of BBEs shows that τ_{BB} follows the relationship[30] of $\tau_{BB} = \tau_0(n_{sc} + 1)^{3/2} n_x^2$,

where the monomer relaxation time, $\boldsymbol{\tau_0}$, is 6.55E-9 s (**Figure S11**). For the linear networks, the characteristic relaxation time, $\boldsymbol{\tau_{lin}}$, varies from 2.66E-4 s to 8.22E-3 s (**Table S7**).

From simple scaling analysis, $\boldsymbol{\tau}$ and $\boldsymbol{v^*}$ should be related by a length scale, $\boldsymbol{l}$, over which the dominant viscous relaxation mechanisms control the separation dynamics of the elastomer-glass interface. **Table 1** provides these values for both the BBEs and linear networks. We find that the length scale of dissipative processes is similar for BBEs (1.44 – 11.44 nm) and linear networks (1.13 – 17.75 nm), varying with the crosslink density of the network. This finding suggests that the significantly lower adhesion exhibited by the BBEs is not controlled by altering the volume over which dissipation acts but rather by altering the intrinsic magnitude of the dissipative mechanisms. In the BBEs, these dissipation mechanisms are attributed to the intrinsic relaxation times of the monomer, $\boldsymbol{\tau_0}$, which can be accessed in the extended side chain configuration. This hypothesis provides insight with regard to the future design of BBEs, especially in the context of controlling adhesion. In particular, this finding suggests that the side chain chemistry and length can play a primary role in tuning the magnitude of rate-dependent dissipative mechanisms for BBEs adhesives.[13, 16] This approach should help to make the adhesive design more direct and

efficient.

Table 1. Scaling analysis for BBEs and linear chain networks. Length scales of energy dissipation, l, were calculated by relaxation times of networks, τ, multiplied with v^*.

BBEs	E (kPa) [a]	tan δ [b]	τ_{BB} (sec) [c]	v^* (μm/sec)	l (nm) = $\tau_{BB} \cdot v^*$
n_x = 17	93.0±5.8	0.020±0.008	1.83±0.20 E-5	77.74±12.17	1.44±0.38
n_x = 25	38.3±1.9	0.022±0.011	1.12±0.13 E-4	32.55±4.03	3.68±0.88
n_x = 34	16.9±0.5	0.036±0.001	4.19±0.35 E-4	27.13±3.11	11.44±2.25
Linear	E (kPa) [a]	tan δ [b]	τ_{lin} (sec) [d]	v^* (μm/sec)	l (nm) = $\tau_{lin} \cdot v^*$
Syl 40	67.7±5.3	0.187±0.001	2.66±1.46 E-4	4.11±0.40	1.13±0.71
Syl 50	23.2±3.5	0.292±0.004	9.96±1.39 E-4	3.65±0.35	3.67±0.86
Syl 55	11.1±1.6	0.369±0.009	8.22±9.69 E-3	2.01±0.19	17.75±21.07

a. E were determined from CAT measurements when the displacement rate is 10 μm/sec.

b. tan δ were determined from DMA measurements **(Figure 5)** when the strain rate is 1 Hz.

c. τ_{BB} were determined from time-temperature superposition plots of DMA measurements (**Figure S10 and Table S6**).

d. τ_{lin} were determined by extrapolations of DMA measurements (**Figure S9 and Table S7**).

4. Conclusions

PDMS BBEs are promising soft materials with properties well-controlled by their molecular architectures and not reliant upon complex formulations with "free", or noncrosslinked, components. Our findings, based on JKR contact adhesion test, demonstrate that the adhesion of PDMS BBEs to glass surfaces can be significantly less than interfaces between glass and linear PDMS networks with similar elastic moduli. The critical energy release rate for initiating interfacial separation, G_0, was found to be independent of the crosslink density of the BBEs, suggesting that this property can be systematically controlled by the monomer chemistry and side chain architecture. After initiation, the BBEs-glass interfaces exhibited velocity-dependent G_c similar to interfaces formed with the linear network elastomers, albeit with magnitudes significantly less. Scaling analysis suggested that the significantly lower G_c for BBEs was

attributed to the magnitude of the dissipative relaxation processes, tan δ, within the BBEs architecture and not the volume over which these processes act. This insight, enabled by the careful analysis of CAT measurements, suggests that the adhesion properties of BBEs can be finely tuned through the monomer chemistry and side chain length, thus offering a robust framework for widely tuning the adhesion of soft materials without time-consuming, complex formulation cycles. Future studies exploring a wider range of side chain monomer chemistry, along with the development of new theoretical models, will help to confirm these findings and provide systematic approaches for controlling adhesion with BBE materials. This approach for soft materials design will have important implications in the design of reversible pressure-sensitive adhesives, as well as other technologies such as robotic gripping devices and energy-dissipative composites.

Author contributions

H.K.: conceptualization, data curation, investigation, writing – original draft; J.J.W.: supervision, funding acquisition, writing – review & editing; A.J.C.: conceptualization, methodology,

supervision, funding acquisition, writing – review & editing.

Authors information

Hyemin Kim − Department of Polymer Science and Engineering, University of Massachusetts Amherst, Amherst, Massachusetts 01003, United States, orcid.org/0009-0003-2444-4079

James J. Watkins − Department of Polymer Science and Engineering, University of Massachusetts Amherst, Amherst, Massachusetts 01003, United States; orcid.org/0000-0001-8302-825X

Alfred J. Crosby − Department of Polymer Science and Engineering, University of Massachusetts Amherst, Amherst, Massachusetts 01003, United States; orcid.org/0000-0001-8850-8869

Conflicts of interest

There are no conflicts to declare.

Acknowledgments

This research was funded by the Army Research Lab's (ARL) National Center for Manufacturing Science (NCMS) Award ID# HQ00341520007 and the Army Research Lab's Award ID# W911NF2120208. Facilities used during the conducting of this research are maintained by the University of Massachusetts Amherst.

References

1. M. Vatankhah-Varnoosfaderani, W. F. Daniel, A. P. Zhushma, Q. Li, B. J. Morgan, K. Matyjaszewski, D. P. Armstrong, R. J. Spontak, A. V. Dobrynin and S. S. Sheiko, *Advanced Materials*, 2017, **29**, 1604209.
2. V. G. Reynolds, S. Mukherjee, R. Xie, A. E. Levi, A. Atassi, T. Uchiyama, H. Wang, M. L. Chabinyc and C. M. Bates, *Materials Horizons*, 2020, **7**, 181-187.
3. T. T. Duncan, E. P. Chan and K. L. Beers, *ACS Applied Materials & Interfaces*, 2019, **11**, 45310-45318.
4. M. Vatankhah-Varnosfaderani, W. F. Daniel, M. H. Everhart, A. A. Pandya, H. Liang, K. Matyjaszewski, A. V. Dobrynin and S. S. Sheiko, *Nature*, 2017, **549**, 497-501.
5. K. Jung, N. Corrigan, E. H. Wong and C. Boyer, *Advanced Materials*, 2022, **34**, 2105063.
6. H. Liang, Z. Cao, Z. Wang, S. S. Sheiko and A. V. Dobrynin, *Macromolecules*, 2017, **50**, 3430-3437.
7. H. Liang, B. J. Morgan, G. Xie, M. R. Martinez, E. B. Zhulina, K. Matyjaszewski, S. S. Sheiko and A. V. Dobrynin, *Macromolecules*, 2018, **51**, 10028-10039.
8. H. Liang, Z. Wang, S. S. Sheiko and A. V. Dobrynin, *Macromolecules*, 2019, **52**, 3942-3950.
9. H. Liang, S. S. Sheiko and A. V. Dobrynin, *Macromolecules*, 2018, **51**, 638-645.
10. S. S. Sheiko and A. V. Dobrynin, *Macromolecules*, 2019, **52**, 7531-7546.
11. M. Maw, B. J. Morgan, E. Dashtimoghadam, Y. Tian, E. A. Bersenev, A. V. Maryasevskaya, D. A. Ivanov, K. Matyjaszewski, A. V. Dobrynin and S. S. Sheiko, *Macromolecules*, 2022, **55**, 2940-2951.
12. L. H. Cai, T. E. Kodger, R. E. Guerra, A. F. Pegoraro, M. Rubinstein and D. A. Weitz, *Advanced*

Materials, 2015, **27**, 5132-5140.

13. K. R. Shull, D. Ahn, W. L. Chen, C. M. Flanigan and A. J. Crosby, *Macromolecular Chemistry and Physics*, 1998, **199**, 489-511.
14. A. J. Crosby and K. R. Shull, *Journal of Polymer Science Part B: Polymer Physics*, 1999, **37**, 3455-3472.
15. A. J. Crosby, K. R. Shull, H. Lakrout and C. Creton, *Journal of Applied Physics*, 2000, **88**, 2956-2966.
16. K. R. Shull, *Materials Science and Engineering: R: Reports*, 2002, **36**, 1-45.
17. B. R. Clarke, H. Kim, M. Ilton, J. J. Watkins, A. J. Crosby and G. N. Tew, *Macromolecules*, 2022, **55**, 10312-10319.
18. S. Wartewig, G. Helmis and M. Klüppel, 1992.
19. C. Tsenoglou, *Macromolecules*, 1989, **22**, 284-289.
20. M. A. Villar and E. M. Vallés, *Macromolecules*, 1996, **29**, 4081-4089.
21. W. F. Daniel, J. Burdyńska, M. Vatankhah-Varnoosfaderani, K. Matyjaszewski, J. Paturej, M. Rubinstein, A. V. Dobrynin and S. S. Sheiko, *Nature materials*, 2016, **15**, 183-189.
22. J. D. Glover, C. E. McLaughlin, M. K. McFarland and J. T. Pham, *Journal of Polymer Science*, 2020, **58**, 343-351.
23. E. M. Thomas, H. Fu, R. C. Hayward and A. J. Crosby, *Soft Matter*, 2022, **18**, 8098-8105.
24. D. Maugis, *J. Phys. D: Appl. Phys*, 1989, **11**.
25. D. Ahn and K. R. Shull, *Langmuir*, 1998, **14**, 3637-3645.
26. D. Ahn and K. R. Shull, *Macromolecules*, 1996, **29**, 4381-4390.
27. A. Gent and J. Schultz, *The Journal of Adhesion*, 1972, **3**, 281-294.
28. S. Bistac, *Journal of colloid and interface science*, 1999, **219**, 210-211.
29. X. Li, S. L. Prukop, S. L. Biswal and R. Verduzco, *Macromolecules*, 2012, **45**, 7118-7127.
30. Z. Cao, W. F. Daniel, M. Vatankhah-Varnosfaderani, S. S. Sheiko and A. V. Dobrynin, *Macromolecules*, 2016, **49**, 8009-8017.